J. Biomater. Sci. Polymer Edn, Vol. 9, No. 7, pp. 681–711 (1998)

Heterogeneous PHPMA hydrogels for tissue repair and axonal regeneration in the injured spinal cord

S. WOERLY [1,*], E. PINET [1], L. DE ROBERTIS [1], M. BOUSMINA [2], G. LAROCHE [3], T. ROITBACK [4], L. VARGOVÁ [4] and E. SYKOVÁ [4]

[1] *Organogel Canada Ltd, 1400 Blvd. du Parc Technologique, Quebec City (Quebec), G1P 4R7 Canada*
[2] *Department of Chemical Engineering, Laval University, Quebec City (Quebec), G1K 7P4 Canada*
[3] *Quebec Biomaterial Institute, Quebec City (Quebec), G1L 3L5 Canada*
[4] *Department of Neuroscience, 2nd Medical Faculty, Charles University, and Institute of Experimental Medicine, Academy of Sciences of the Czech Republic, Prague, Czech Republic*

Received 12 June 1997; accepted 14 January 1998

Abstract—A biocompatible heterogeneous hydrogel of poly[*N*-(2-hydroxypropyl) methacrylamide] (PHPMA) showing an open porous structure, viscoelastic properties similar to the neural tissue and a large surface area available for cell interaction, was evaluated for its ability to promote tissue repair and axonal regeneration in the transected rat spinal cord. After implantation, the polymer hydrogel could correctly bridge the tissue defect, form a permissive interface with the host tissue to favour cell ingrowth, angiogenesis and axonal growth occurred within the microstructure of the network. Within 3 months the polymer implant was invaded by host derived tissue, glial cells, blood vessels and axons penetrated the hydrogel implant. Such polymer hydrogel matrices which show neuroinductive and neuroconductive properties have the potential to repair tissue defects in the central nervous system by promoting the formation of a tissue matrix and axonal growth by replacing the lost of tissue.

Key words: Hydrogel; rheology; porosimetry; infrared spectroscopy; scanning electron microscopy; neural tissue; immunocytochemistry; spinal cord; regeneration.

INTRODUCTION

Tissue destruction or tissue loss of the central nervous system (CNS), resulting from elective surgery such as oncological surgery or resection of scarring or necrotic tissue, is associated with interruption of axonal pathways and clinical functional deficits. For example, severe injury of the spinal cord results in the formation of complex scar tissue that prevents regenerating axons to traverse the lesion, resulting

*To whom correspondence should be addressed. E-mail: woerlyst@organogel.com

in paraplegia and tetraplegia [1], and inducing axon of spinal tracts to regenerate requires first to remove the scarring tissue. Reconstruction of damaged parts of the CNS would therefore require methods to be developed to reform a tissue structure into an integrated tissue-to-organ with the various CNS cell constituents that include glia cells, mesenchymal cells, blood vessels, extracellular matrix components, and regenerated nerve fibres. This is because in most vertebrates including human, the capacity for regeneration in the CNS is very limited [2], and restoration of a tissue framework and axonal pathways of the white and grey matter at the end-point cannot be achieved [3, 4]. To overcome this problem, cell and tissue grafts have been investigated for more than a century to replace tissue in the lesioned CNS, both at the experimental and clinical level [5, 6]. Thus, syngenic autograft or homograft, allograft or xenograft, such as foetal neural tissue [7] Schwann cells and sensory neurones [8] and immature astrocytes [9] have been transplanted into the lesioned CNS. A new approach is being developed for restoration of lost cells in the CNS which use isolated precursors of neural tissue cells [10], genetically modified donor cells [11], and immortalized cell lines [12]. Peripheral nerve segments including cultured non-neuronal cells [13] or embryonic neural tissue cells [14] have also been grafted. Natural polymer matrices have shown to be useful in the reconstructive approach of the CNS tissue, such as collagen matrices [15, 16] containing neuroactive agents [17, 18], or including neural grafts [19], Schwann cells [20], or composite collagen matrices [21]. More recently, synthetic biomaterials have been used as an attempt to induce cell and tissue growth in the injured CNS, including nitocellulose membranes [22], tubes of poly(acrylonitrile–vinylchloride), alone [23] or modified with poly(ethylene oxide) [24], tubes of polycarbonate [25, 26] or of nitrocellulose [27] and biodegradable polylactide implants [28].

An entirely new approach to promote tissue repair in the CNS involves the use of synthetic polymer hydrogels as support matrices to help regenerate tissue structure from the cellular post-injury response [29–32]. Hence, in contrast to current cell and tissue grafting technology, this approach is based on tissue repair by manipulating the healing process of the wound in such a way as to promote the formation of a new tissue structure within the polymer matrix. Hydrogels are water-swollen networks of hydrophilic homopolymers or copolymers and are currently utilized for a variety of biomedical applications [33]. Properties of hydrogels such as permeability to small molecules, viscoelastic behavior, low interfacial tension with biological fluids and stability make these materials suitable for implantation in soft tissue [34]. In addition, the design of macromolecular structures with physical properties needed for establishing a permissive interface, mobilizing the host's tissue cells, and stimulating tissue remodelling without mechanical injury at the host tissue interface are required when hydrogels are being contemplated for tissue replacement. Thus, a large specific surface areas available for cell interactions, a high fractional porosity of hydrogels and mechanical properties that match those of the host tissue are favourable characteristics for promoting tissue ingrowth into the hydrogel structure. In addition, pore size distribution and communication between

pores are important structural properties for cell loading and tissue expansion within the polymer matrix. These structural properties are controlled by the polymerisation process of the molecular subunits [35, 36].

This paper presents results of a heterogeneous poly[*N*-(2-hydroxypropyl)methacrylamide] (PHPMA) hydrogel with defined porosity and mechanical properties for promoting tissue repair and axonal regeneration in the CNS. The PHPMA hydrogel was characterized for its porous structure, diffusion and mechanical properties, and network topology. This polymer hydrogel was evaluated in the transected spinal cord for its capacity to bridge between the cut ends of transected spinal cord, and to provide a substrate for tissue ingrowth, angiogenesis, and axonal regeneration. Our results show that the PHPMA hydrogels can correctly bridge the tissue defect created in the spinal cord, initiate tissue formation and axonal regeneration without the addition of exogenous neuroactive factors, resulting in improvement of locomotor functional recovery in some animals.

METHODS

Preparation of PHPMA hydrogels

Macroporous hydrogels were prepared from *N*-(2-hydroxypropyl)methacrylamide (HPMA) (synthesis of HPMA was previously described, see ref. [37]) by heterophase separation using radical polymerization in a pore-forming solvent with a divinyl cross-linking agent. The reaction was carried out in sealed nitrogen atmosphere ampoules. After polymerization, the xerogels were removed from the ampoules and were allowed to swell in ethanol. The white spongy hydrogels were washed with distilled water. The eluates leached out of the gels were exchanged for fresh water every day for 2 weeks. All procedures were carried out in a flow cabinet. The eluates were concentrated by vacuum evaporation at 60°C and separated by HPLC on a Waters LCM1 + system using NovaPack-C18 (Waters) analytical reverse phase column with methanol/water 25/75 at 1 ml min^{-1} with an absorption detection at $\lambda = 210$ nm. The decrease of the monomer leached out of the gels was quantified from the chromatogram peak area using HPMA standard samples.

Characterisation of PHPMA hydrogels

Equilibrium water content (EWC). Gel disks were equilibrated in deionized water at room temperature for 1 week. The gels were blotted with laboratory tissue (to remove surface water), weighed, dried under vacuum at room temperature, and weighed again. The swelling capacity was determined as the mass ratio of water to swollen gel according to the equation:

$$\frac{W_s - W_d}{W_s} \times 100,$$

where W_s is the weight of the swollen gel and W_d the weight of the dried gel. Swelling was calculated as the mean of at least five measurements of different gel samples.

Scanning electron microscopy. The structure of the gel was examined by scanning electron microscopy after drying the gel using 1,1,1,3,3,3-hexamethyldisilazane (HMDS) [38]. The swollen gel was dehydrated through a graded series of ethanol solutions of 70, 85, 95, and 100% for 30 min each. The gel was then immersed in HMDS and air dried in a flow cabinet at room temperature. The dried gel was fractured using an razor blade and was mounted on stubs with colloidal graphite and sputter-coated with gold to an approximate thickness of 200 Å. The surface and the bulk of gels were examined with a Jeol T 300 scanning electron microscope using an accelerating voltage of 15 kV.

Mercury porosimetry. The porosity (pore size distribution and cumulative intruded pore volume) and surface area were determined by mercury porosimetry using a PoreSizer 9329 (Micromeritics) both with a low-pressure and a high-pressure regime. The porosity was measured on freeze-dried samples and the pore diameter, D, was calculated using the Washburn equation [39]:

$$\mathrm{D} = -\frac{4\gamma \cos\theta}{P}, \tag{1}$$

where P is the applied pressure, θ the contact angle (130 deg) and γ the surface tension (485 dyn cm^{-1}) of mercury. The intrusion volume was recorded for pressure ranging from 0 to 30 000 psia. The intrusion is the ratio of the injected mercury volume to the volume of the gel. Cumulative intrusion and pore size (log differential intrusion) distribution were plotted on semilogarithmic co-ordinates. Porosity was calculated using the equation:

$$\frac{d_s - d_b}{d_s} \times 100,$$

where d_s is the skeletal density of the dried gel (derived from gel volume with exclusion of the volume of the samples's pore structure) and d_b is the bulk density of the dried gel (derived from gel volume that includes the volume of the sample's pore structure).

Surface area (i.e. pore wall surface) was computed on the basis of the applied pressure vs intruded volume of mercury using the following equation [40]:

$$A = -\frac{\int_0^{V_{max}} P \, dV}{\gamma \cos\theta}. \tag{2}$$

In order to determine the pore distribution domains of the hydrogel, the critical pressure P_c, i.e. the minimum pressure required to intrude the largest pore, was

determined using the following equation [41]:

$$\ln\left[V(\infty) - V(P)\right] = \ln\left[V(\infty) - V(P_c)\right] - m\left[\ln(P) - \ln(P_c)\right], \quad (3)$$

where $V(\infty)$ is the volume of intruded mercury at the maximum intrusion pressure and $V(P)$ the volume of intruded mercury at pressure P, and m is the slope of the graph.

Rheological measurement. Mechanical properties were measured for both the PHPMA hydrogel and recently sliced rat brain samples. Due to their weak mechanical properties (low modulus) and their sensitive structure, the materials were tested in a dynamic regime at small amplitudes of deformation.

Small-amplitude oscillatory shear measurements were carried out on a Bohlin-CVO constant stress rheometer in parallel-plate geometry. A special cylindrical cell with a serrated bottom plate was designed to run measurements in a liquid environment. The sample (hydrogel or neural tissue) was cut into disks of 15 mm in diameter and 1.3 mm in thickness and then introduced in the cylindrical cell and slightly compressed by the upper serrated plate to create a fixed gap. A gap of 1.1 mm was chosen to compare the mechanical properties of the gel and the rat brain. In addition, successive oscillatory shear measurements were carried out on the gel subjected to compression and decompression cycles. Starting at 1.1 mm, the gel was smoothly compressed to 1.05, 1.0, 0.95, and 0.9 mm and was subjected to oscillatory shear for each gap. After each compression the sample was left for 5–15 min to ensure osmotic equilibrium between the solution and the gel prior to testing. The cell was filled with a saline solution (0.9% NaCl) prior to testing and all experiments were conducted at 37°C. To avoid evaporation of the solution the cylinder was isolated with a Teflon cover. The frequency was varied from 0.01 to 100 rad s^{-1}. Stress sweep measurements were first conducted to delimit the region of linear viscoelasticity, that is the stress, τ^*, is proportional to the strain, γ^*. Depending on the frequency range, the stress was adjusted so that the rheological behavior was linear viscoelastic. Care was taken to impose adequate stresses so that the resulting strains were small enough and did not break the structure of the gel. Oscillatory shear tests were carried out from higher to lower frequencies, and the sample stability was verified by reproducing higher frequency measurements. Each measurement was repeated three times and the accuracy of the reported data is believed to be within $\pm 5\%$. Under small harmonic strains, the ratio of the stress to the strain is independent of the imposed strain [42].

$$G^*(\omega) = \frac{\tau^*(t)}{\gamma^*(t)} = G'(\omega) + iG''(\omega), \quad (4)$$

which means that the stress is a linear function of strain (domain of linear viscoelasticity). $G^*(\omega)$ is the complex shear modulus; $G'(\omega)$ is called the storage

modulus and represents the elastic contribution and $G''(\omega)$ the loss modulus and represents the viscous contribution to the viscoelastic behavior of the material. The complex dynamic viscosity is obtained by the ratio:

$$\eta^*(\omega) = \frac{G^*(\omega)}{i\omega}. \tag{5}$$

Tetramethylammonium (TMA^+) diffusion measurements. TMA^+-selective microelectrodes were used to measure diffusion properties in the hydrogel. The ion-selective microelectrodes for TMA^+ were made from double-barrel tubing as described elsewhere [43]. The ion-exchanger was a Corning 477317, and the ion-sensing barrel was back-filled with 100 mM TMA chloride while the reference barrel contained 150 mM NaCl. Electrodes were calibrated using the fixed-interference method in a sequence of flowing solutions. Calibration data were fitted with the Nikolsky equation to determine electrode slope and interference. The shank of the iontophoresis pipette was bent, so that it could be aligned parallel to that of the ISM. Electrode arrays were made by gluing together an iontophoresis pipette and a TMA^+-selective microelectrode with a tip separation of 140–200 mm. Iontophoresis parameters were a +20 nA bias current (continuously applied to maintain a constant electrode transport number) and a +100 nA current step of 60 s duration to generate a TMA^+ diffusion curve.

TMA^+ diffusion curves were recorded with a PC-based Pentium computer and analysed by fitting the data to a solution of the diffusion equation [44]. TMA^+ concentration vs time curves were first recorded in 0.3% agar gel (Agar Noble, Difco, Detroit, MI, USA) made up in 150 mM NaCl, 3 mM KCl and 1 mM TMA^+. The diffusion curves in agar were used to determine the electrode transport number, n, and free TMA^+ diffusion coefficient, D ($cm^2\ s^{-1}$). Diffusion curves were then recorded in a non-implanted hydrogel or in the brain and analysed to yield a value of α, the TMA^+ apparent diffusion coefficient in gel, ADC_{TMA} ($cm^2\ s^{-1}$), λ and non-specific TMA^+ uptake, k' (s^{-1}). Volume fraction (α) is the restricted volume of the tissue or hydrogel which is available for diffusion. Tortuosity is the effective path length for diffusion of particles between two points due to various obstacles in the tissue or hydrogel which slow down the diffusion of molecules. It is a geometrical factor calculated as $= (D/ADC_{TMA})^{0.5}$. These parameters were extracted by a nonlinear curve-fitting simplex algorithm operating on the diffusion curve described by Eq. (6), which represents the behavior of TMA^+, assuming that it spreads out with spherical symmetry, when the iontophoresis current is applied for duration S [44]. In this expression, C is the concentration of TMA^+ at time t and distance r. The equation governing diffusion is:

$$C = G(t) \qquad t < S \text{ for the rising phase of the curve,}$$
$$C = G(t) - G(t - S) \qquad t > S \text{ for the falling phase of the curve.}$$

The function $G(u)$ is evaluated by substituting t or $t - S$ for u in the following equation:

$$G(u) = \left(Q\lambda^2/8\pi D\alpha r\right)\{\exp\left[r\lambda(k'/D)^{1/2}\right]\mathrm{erfc}\left[r\lambda/2(Du)^{1/2} + (k'u)^{1/2}\right] + \exp\left[-r\lambda(k'/D)^{1/2}\right]\mathrm{erfc}\left[r\lambda/2(Du)^{1/2} - (k'u)^{1/2}\right]\}. \quad (6)$$

The quantity of TMA^+ delivered per second is $Q = In/zF$, where I is the step increase in current applied to the iontophoresis electrode, n is the transport number, z is the number of charges associated with substance iontophoresed (+1 here) and F is Faraday's electrochemical equivalent. The function 'efrc' is the complementary error function. When the experimental medium is agar, by definition, $\alpha = 1 = \lambda$ and $k' = 0$, and the parameters n and D are extracted by curve fitting. Knowing n and D, the parameters α, λ (D free solution/ D in hydrogel) and k' can be obtained.

Implantation study

The hydrated polymer gels were sterilized in boiling water. Twenty Sprague Dawley rats (200–250 g) were used. The animals were anesthesized by an intraperitoneal injection of ketamine hydrochloride (87 mg ml^{-1}) and xylazine (13 mg ml^{-1}). Using aseptic surgical techniques, the animals underwent a laminectomy at the thoracic level T9 as previously described [15]. The exposed spinal cord was thoroughly irrigated with a cold saline solution prior to transection. A cordotomy was performed using microscisors, and a 2-mm spinal tissue segment was removed. Following spontaneous hemostasis, excess clot was washed from the cavity with a chilled saline solution. The hydrogel implant was sized to adapt to the dimension and shape of the cavity and was inserted into the lesion cavity ensuring a complete apposition of the polymer surface with the surfaces of the spinal stumps (this was verified under the surgical microscope at high magnification). The muscles were sutured and the skin closed with wound clips. After surgery the rats received an intramuscular injection of penicillin G (10 000 U) and a subcutaneous injection of an antalgic (buprenorphine, 0.05 mg kg^{-1}). Bladder expression was performed twice a day until recovery of sphincter control. During the first week, the rats were given tetracycline in drinking water to prevent urinary tract infection. The animals were observed daily for spontaneous recovery of locomotor activity and postural functions of their hindlimbs during overground locomotion.

Tissue processing

The animals were allowed to survive from 3 days to 20 weeks (Table 1). The animals were anaesthetised and perfused through the heart with a phosphate buffer saline (PBS) containing heparin followed with paraformaldehyde (4% solution in 0.1 M PBS). The spinal cords were removed and transferred to PBS–sucrose 30% for 24 h. After rincage in PBS, 1 cm tissue blocks including the gel implant were embedded in egg yolk that was allowed to harden with formalin vapour. The blocks were cut into 40-μm thick frozen horizontal sections for immunostaining with the following

Table 1.
Numbers of animals at the different survival times

Survival	No.	Experimental groups
3 days	1	Hydrogel implant
1 week	5	Hydrogel implant[a]
5 weeks	2	Hydrogel implant
5 weeks	2	Control transection
12 weeks	6	Hydrogel implant[a]
12 weeks	2	Control transection
20 weeks	5	Hydrogel implant[a]
Total	23	

[a] Animals were lost which were not used for morphological studies.

antibodies: Glial Fibrillary Acidic Protein (GFAP, Dako, 1 : 100), neurofilaments 200 (Sigma, 1 : 75), and fibronectin (1 : 100). The sections were washed 3 × 10 min in Dulbecco's phosphate buffered saline (DPBS) containing 0.1% bovine serum albumin (BSA, Sigma) and 0.2% Triton, then pre-incubated at room temperature for 30 min with 1% swine serum (Laval University) or 1% rabbit serum (Sigma). Sections were incubated with the appropriate antibodies diluted in DPBS-BSA-Triton, and after washing in DPBS (3 × 10 min), sections were further incubated with anti-rabbit TRITC (1 : 30) or anti-mouse TRITC (1 : 30) at room temperature for 3 h. The sections were washed again in DPBS (3 × 10 min) and mounted onto subbed slides and coverslipped using Citifluor. Additional sections were processed for silver impregnation using the Holmes technique.

Image analysis

The implantation site was characterized quantitatively. Eleven horizontal tissue sections were selected to be examined with a 10 × objective through the largest transverse diameter of the cord of spinal cords ($n = 6$) to visualize in bright field the entire implantation site, using a CCD video camera attached to a Nikon microscope and a high resolution Trinitron monitor. The images were digitized and image analysis measurements were performed at constant microscope settings with a Bioquant System. The total area of implant, the perimeter of the polymer that interfaces with the host tissue were determined.

Scanning electron microscopy

Three-month explanted hydrogels were viewed under scanning electron microscopy. The spinal cord containing the gel implants were fixed in 2.5% glutaraldehyde, washed and postfixed in osmium tetroxide (1%) for 2 h, and dehydrated through a graded series of ethanol. The samples were dried using HMDS and processed for scanning microscopy as described above.

Attenuated total reflection–Fourier transform infrared (ATR-FTIR) spectroscopy

Three month-explanted hydrogels, fixed spinal cord tissue and non implanted hydrogels (control) were analysed by ATR-FTIR. Infrared (IR) spectra were recorded with a Nicolet Magna-550 Fourier transform infrared spectrometer with a DTGS detector and a germanium coated KBr beamsplitter. Two hundred and fifty scans were acquired with an optical retardation of 0.25 cm, triangularly apodized and Fourier transformed to yield a 4-cm^{-1} resolution. The attenuated total reflectance (ATR) mode was used for recording the infrared spectra of the hydrogel samples with a Split Pea attachment (Harrick Scientific Corporation) equipped with a Si hemispherical, 3 mm diameter internal reflection element (IRE). The IRE is bevelled on the edge of its flat surface to provide a sampling area slightly larger than the 150–200 μm diameter hot spot on the crystal.

RESULTS

Hydrogel characteristics

The hydrogels were opaque and the water fraction represented 95.66% of the swollen weight of the hydrogel. The high water content and the high fractional porosity of the PHPMA hydrogel were also confirmed by thermogravimetry (not shown) and porosimetry (*vide infra*). Under scanning electron microscopy the PHPMA gels demonstrate a macrophase separated structure. The bulk of the gel constituted a colloidal-type structure forming a three-dimensional network of microspheres of 3–5 μm in loosely-packed contact (Fig. 1A). The limit of the pore system was represented by the contiguity of the surface of the spheres, while the effective surface area of the hydrogel was a function of the mesopores present at the surface of the spheres (Fig. 1B). The voids constituted an extensive open interconnected pore system corresponding to non-circular macropores delimited by the surface of the spheres, while the geometry and the topology of the pore space was represented by the spatial arrangement of the sphere network.

Diffusion measurements showed that TMA^+ diffusion parameters — volume fraction α and tortuosity λ — in hydrogels differ from those in diluted agar gel where there is a free diffusion and, therefore, $\alpha = 1 = \lambda$ and $k' = 0$. In polymer hydrogels the mean values (mean $\pm$ SEM, $n = 14$, at 20°C) were: $\alpha = 0.80 \pm 0.013$ ($p_2 < 0.0001$), $\lambda = 1.13 \pm 0.008$ ($p_2 < 0.0001$) and $k' = 8.48 \times 10^{-6}$ $cm^2\,s^{-1}$. It is, therefore, evident that the diffusion of a rather small molecule such as TMA^+ (molecular mass of 74 Da) is more hindered in polymer hydrogels than in diluted agar. The diffusion of small molecules is however much less hindered than in nervous tissue where typical values of $\alpha = 0.20$ and of $\lambda = 1.5$ [45].

Figure 2 shows the rate of release of HPMA compounds from a xerogel–hydrogel system in ethanol and in water. Most of the low molecular weight compounds were washed out within 5 days. After 3 days, 98% of total unreacted HPMA and oligomers were removed as well as unreacted and decomposition products of

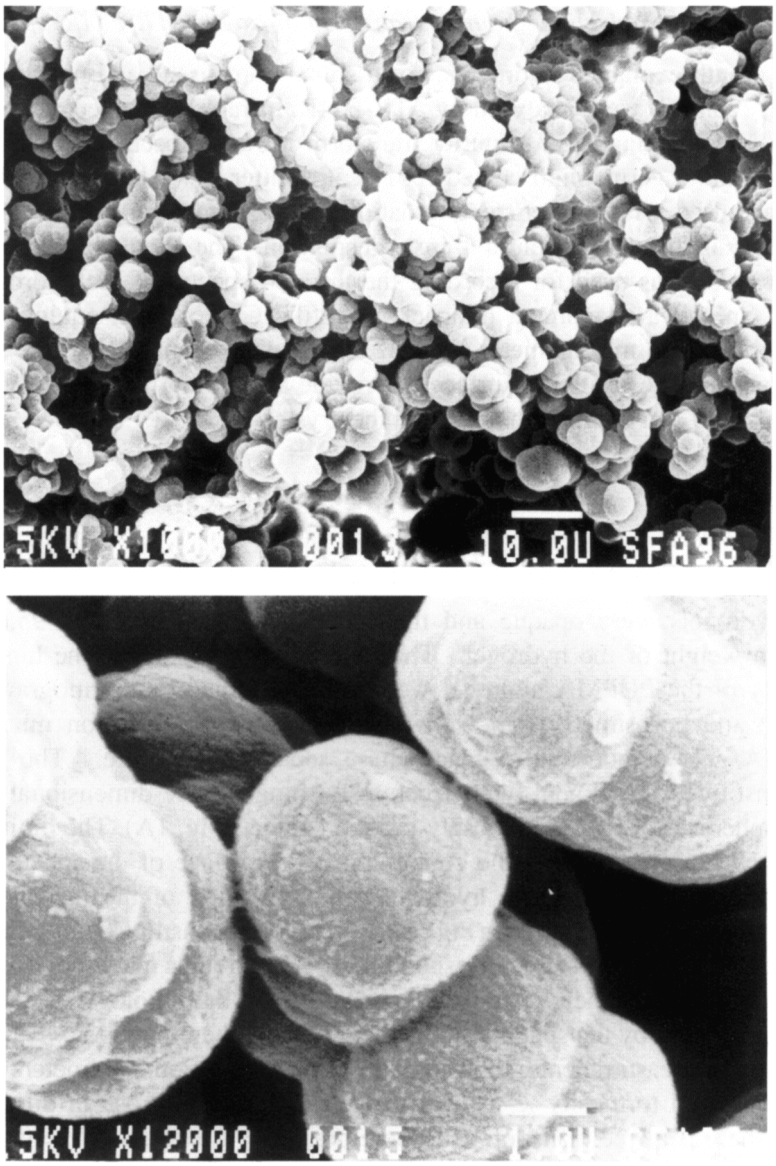

Figure 1. (A) Scanning electron microscopy micrograph of a cross-section of a PHPMA hydrogel showing the structure of the macromolecular network constituted by cross-linked polymer microspheres of 3–5 μm in diameter and the associated porous structure. (B) High power scanning electron microscopy of the PHPMA hydrogel showing the 'orange peel' aspect of the surface of the microspheres, corresponding to the mesopore scale.

initiator. After 2 weeks no trace of HPMA compounds could be detected by UV absorption during the HPLC separation. The hydrogels were thus considered free of low molecular weight compounds for implantation.

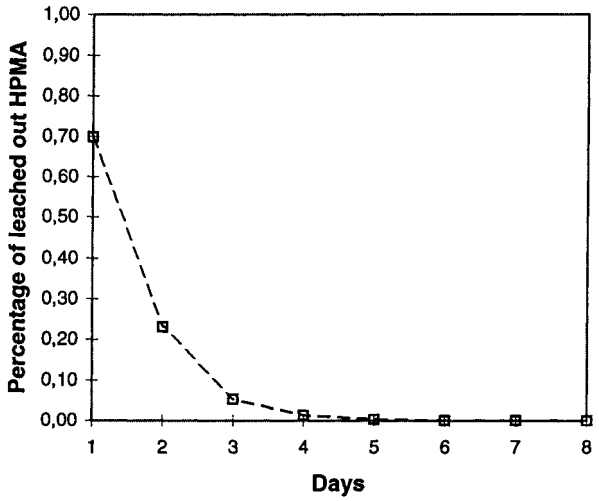

Figure 2. Kinetics of the release of HPMA products from the xerogel–hydrogel system during washing.

Table 2.
Characteristics of the porous structure of the PHPMA hydrogel

	Pore diameter (μm)		
	1–10	10–50	50–300
Pore volume (%)	8.77	78.70	11.47

Pore structure characterization of the PHPMA heterogeneous hydrogels by mercury porosimetry revealed a large void volume (cumulative intruded volume of mercury to the volume of the gel) corresponding to a fractional porosity of 89 ± 2% (n = 46) and a median pore diameter of 22 ± 3 μm (n = 46). The largest fraction of the total pore volume of the gel is occupied by a pore regime of 10–50 μm (Table 2). The pore structure of the hydrogel was defined by the surface of the polymer microspheres, forming an open interconnected porous system. The intrusion curve of mercury (Fig. 3A) shows that the hydrogel was hyperporous from 23 μm (fractional porosity for pores larger than 23 μm and which occupy at least 50% of the gel volume) and macroporous with pores extending up to 300 μm. The sigmoid shape of the intrusion curve indicated that the internal pore structure of the PHPMA gel was fairly homogeneous in macro and mesopore domains, corresponding to a log-normal distribution (Gaussian distribution of the logarithm of diameter) (Fig. 3B). Mercury extrusion from pores upon reduction of pressure indicated the existence of a hysteresis between the intrusion and retraction curves due to the entrapment of mercury within the network (Fig. 3A). Pore wall surface area in the range of macropores and mesopores, up to 0.006 μm, shows a value of 40 ± 8 $m^2 g^{-1}$ (n = 46) (Fig. 3C). There was no significant surface detectable above 30 μm. Figure 3C

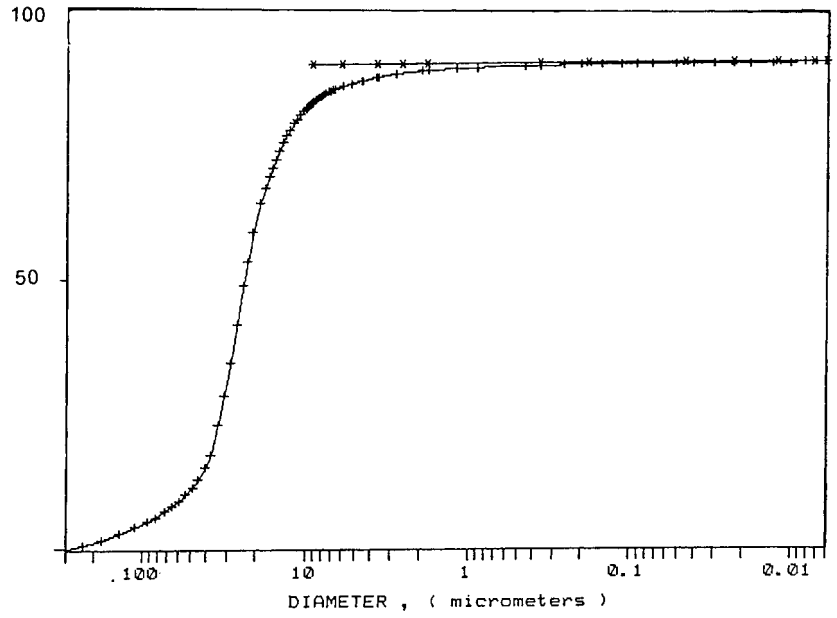

(A)

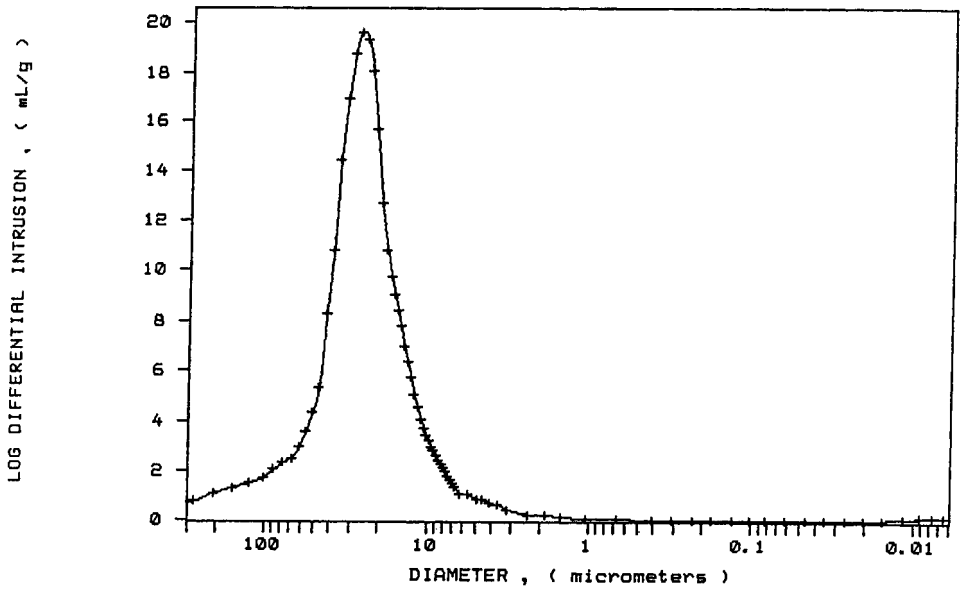

(B)

Figure 3. (A) Mercury porosimetry intrusion–extrusion plots of a PHPMA hydrogel, expressed as a percentage of the intruded–extruded volume of mercury against pore diameter. (B) Plot of pore size distribution (log differential intrusion) against diameter of PHPMA hydrogel. (C) Plot of the cumulative surface pore area of a PHPMA hydrogel against pore diameter. (D) Corrected volume log–log volume plot of a PHPMA gel from intrusion parameters.

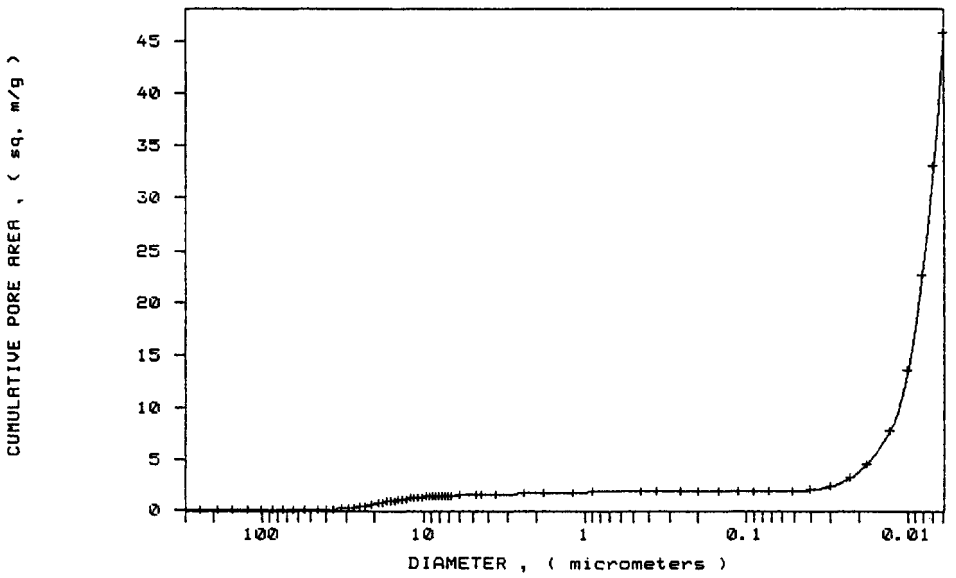

(C)

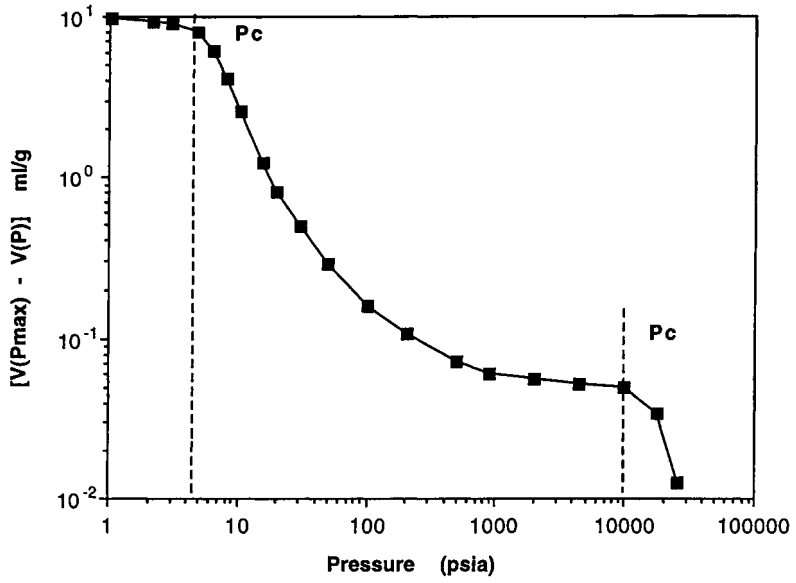

(D)

Figure 3. (Continued).

shows two discontinuities corresponding to an increase of the pore area; at 20 μm and at the upper mesopores (20 nm). The sharp increase of the surface area observed at upper mesopores represented 85% of the total surface of pore area within the range of pores intruded. These results are substantiated in Fig. 3D which shows

the two corresponding critical breakthrough pressures at 5 and 10 000 psia with a sharp decrease in the intrusion slope. This indicates that the hydrogel has two porous domains with two distinct pore distributions; between 5 and 1000 psia and pores intruded between 10 000 and 30 000 psia.

Rheological measurements aimed at characterizing the mechanical behavior of the gel with respect to the CNS tissue, and the intrinsic mechanical properties of the swollen gel network subjected to compression and decompression cycles. The dynamic moduli G' and G'' of the gel are shown in Fig. 4A. The figure shows that the gel typically exhibits a solid-like behavior $G' \gg G''$ [46] with constant elastic modulus ($G' \approx 2600$ Pa). Figure 4B shows the linear viscoelastic functions G^* and η^* of the gel and of the rat brain. This figure shows that the gel and the brain tissue have similar behaviors, that is a constant G^* and an increasing η^* as the frequency is decreasing. Since G^* is constant over the whole frequency range, η^* varies linearly as a function of ω with a slope -1 for both materials (see Eq. 5). A difference in absolute values of G^* and η^* are however observed.

The results of the experiments shown in the previous figures were carried out using the same gap of the gel and the brain in equilibrium with the 0.9% NaCl solution. The question then arises to what extent the solution in contact with the gel may affect its rheological behavior. To clarify this point, successive oscillatory shear measurements were carried out on the same gel at different gaps and the results for the compression/decompression process are shown in Fig. 4C. This figure shows that G^* clearly increases as the gap decreases. This can be explained by the fact that the solution entrapped in the gel slips out by the squeezing flow generated by compression. This for small gaps, the proportion of the solid phase in the swollen network increases, yielding to an increase of the mechanical properties of the gel. The process seems to be reversible. In fact decompression from 0.9 to 1.1 mm by 0.1 mm steps gave similar results as those obtained during compression as evidenced by Fig. 4C. This suggests that the structure of the gel was not disturbed, at least at the sensitivity of the rheometer's transducer, by compression and decompression cycles. Then it is reasonable to assume that the total complex modulus, G^*, of the swollen gel can be written as a function of the complex moduli of the two contributions, G^*_s and G^*_{dg}, as follows:

$$G^* = \varphi G^*_s + (1 - \varphi) G^*_{dg}. \tag{7}$$

G^*_s and G^*_{dg} are the complex moduli of the solution and the dry gel, respectively, φ is the volume fraction of the solution entrapped in the gel and is directly proportional to the gap h ($\varphi = ah$, a being the constant of proportionality). Equation (7) can then be written in the following form:

$$G^* = ah(G^*_s - G^*_{dg}) + G^*_{dg}. \tag{8}$$

The plot of G^* as a function of the gap, h, shown in Fig. 4D confirms that the complex modulus is a linear function of the gap. Thus, extrapolation of $G^*(h)$ at

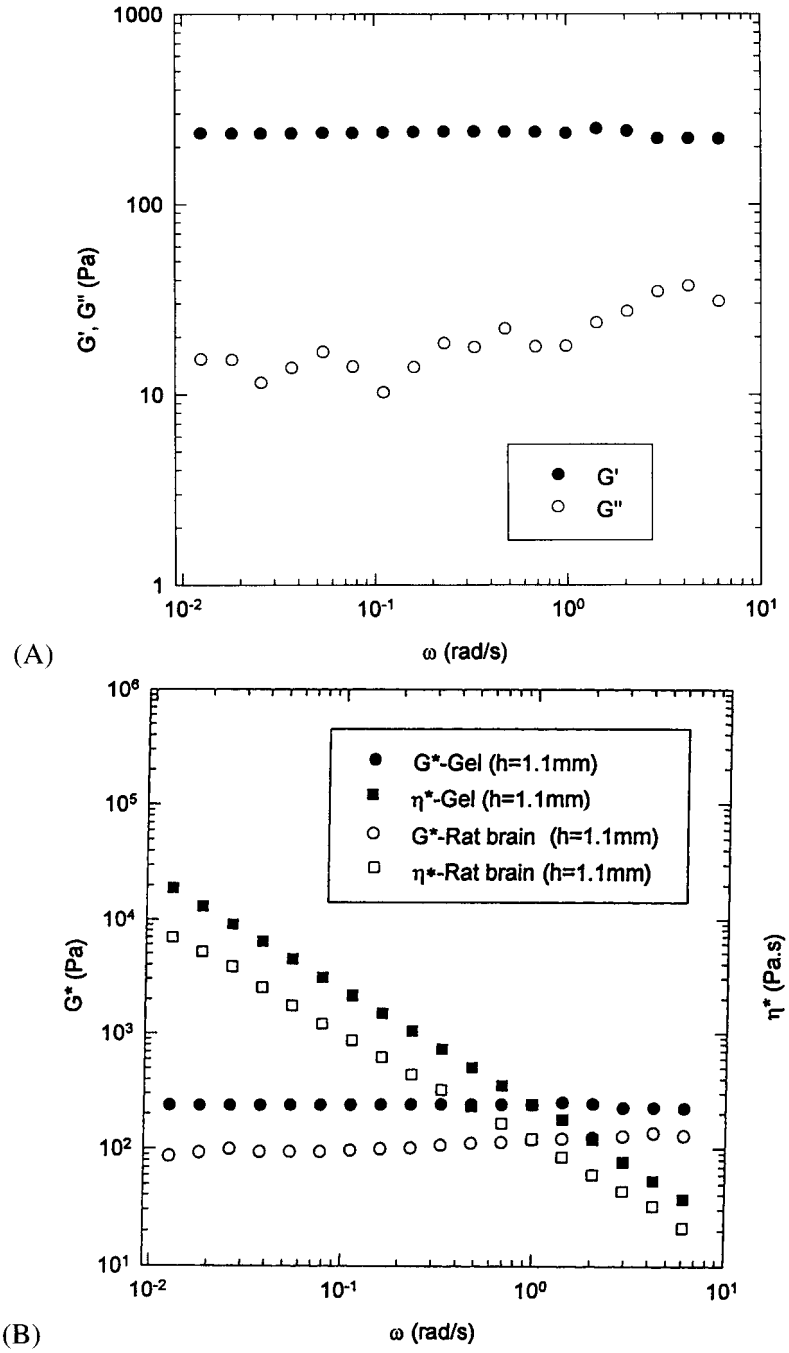

Figure 4. (A) Dynamic moduli, G' and G'', as function of frequency for the PHPMA hydrogel at 37°C. (B) Comparison of linear material functions, G^* and η^*, of the rat brain and the PHPMA hydrogel at 37°C. (C) Complex shear modulus, G^*, of the hydrogel as a function of frequency at different gaps after compression and decompression. (D) Variation of the complex modulus, G^*, of the hydrogel as a function of the gap.

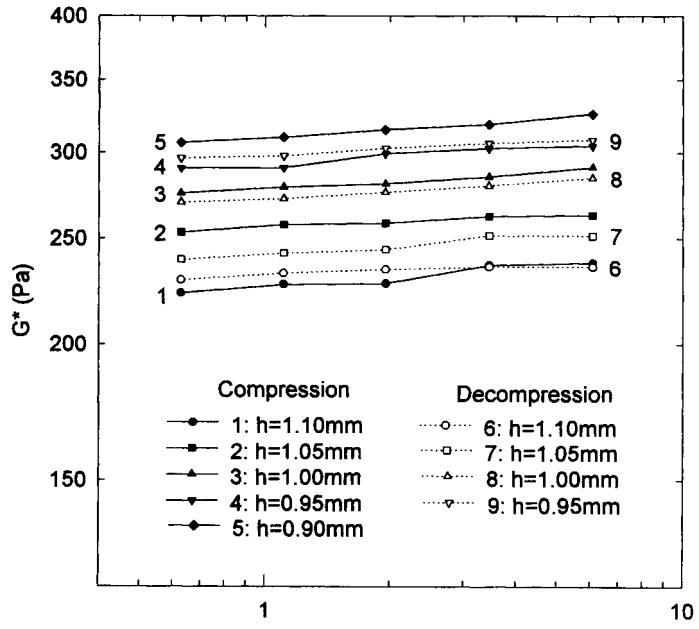

(C)

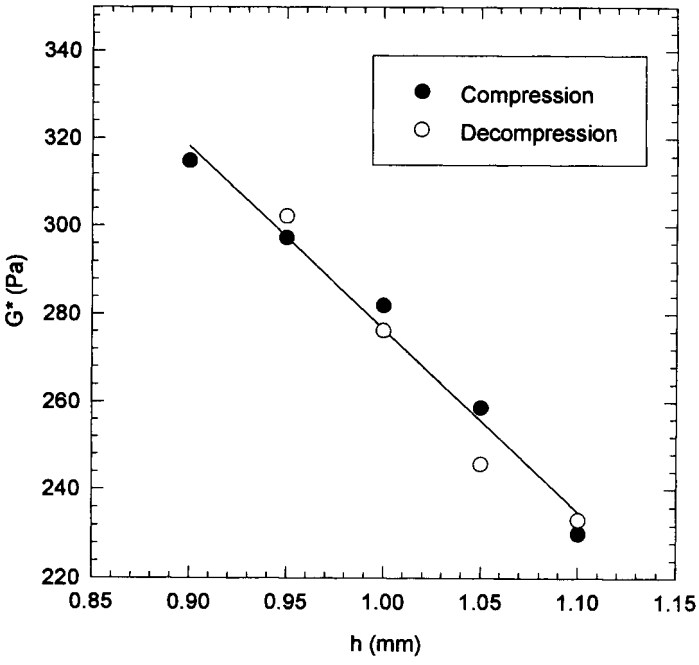

(D)

Figure 4. (Continued).

vanishingly small gaps gives an estimation of the complex modulus of the dry gel which in the present case shows an asymptotic value of 735 Pa. It, however, should be mentioned that extrapolation is an idealization of actual geometry of flow since for completely dry samples, the gap will given by the amount of the dry gel between the two parallel plate fixtures.

PHPMA hydrogel implantation

The transection of the spinal cord severs all elements of the neural tissue, including myelinated axons, neural and glial elements and blood vessels (dorsal and ventral spinal arteries), producing a permanent paraplegia in the rats. The cavity was made after complete transection of the cord at two levels separated by 2 mm and by removing the spinal tissue segment. Clean and straight-line sections of the spinal tissue was facilitated by cooling the spinal cord before lesioning. For each animal, completeness of the lesion was verified visually under the surgical microscope and after control of the hemostasis. A representative sample of the size and shape of the lesion for the implantation of the hydrogel is shown in Table 3. As early as 3 days after surgery, macroscopic examination of the spinal cord showed that the hydrogel implants were found within the spinal cord and formed a complete bridge between the distal and proximal spinal segments (Fig. 5A). Five weeks later, the appearance of the hydrogel had changed and it was difficult to clearly distinguish a sharp interface between the polymer implant and the host tissue as result of the gel integration into the host (Fig. 5B). There was no discontinuity between the polymer surface and the tissue, and the total available surface of the hydrogel merged with the cut surface of the spinal tissue as shown on consecutive adjacent sections. Optimal surgical techniques and an adequate gel placement in the transection site yielded excellent integration of the gel and the absence of cyst formation in the adjacent spinal tissue. The polymer matrices showed a strong bioadhesiveness and this was noticed during the placement of the polymer between the two severed spinal segments; the polymer gel stuck very rapidly and strongly to the cut spinal cord as evidenced by the difficulty of retrieving it after a few seconds without damaging the spinal stump. In contrast, transected spinal cords without gel implantation showed typical pathological changes with massive tissue destruction, microcyst formation and the development of dense scar tissue filling the transection cavity (Fig. 5C). Observations of cross-sectional areas of the water-saturated hydrogels on histological sections as well as a gross examination of the implantation site did

Table 3.
Morphometrics characteristics of the implantation site containing the polymer gel implant ($n = 6$)

Area (mm^2)	Perimeter (mm)	Shape factor[a]
2.86 ± 0.12	8.21 ± 0.16	0.54 ± 0.03

[a] Shape factor: 1 for circle and 0 for line.

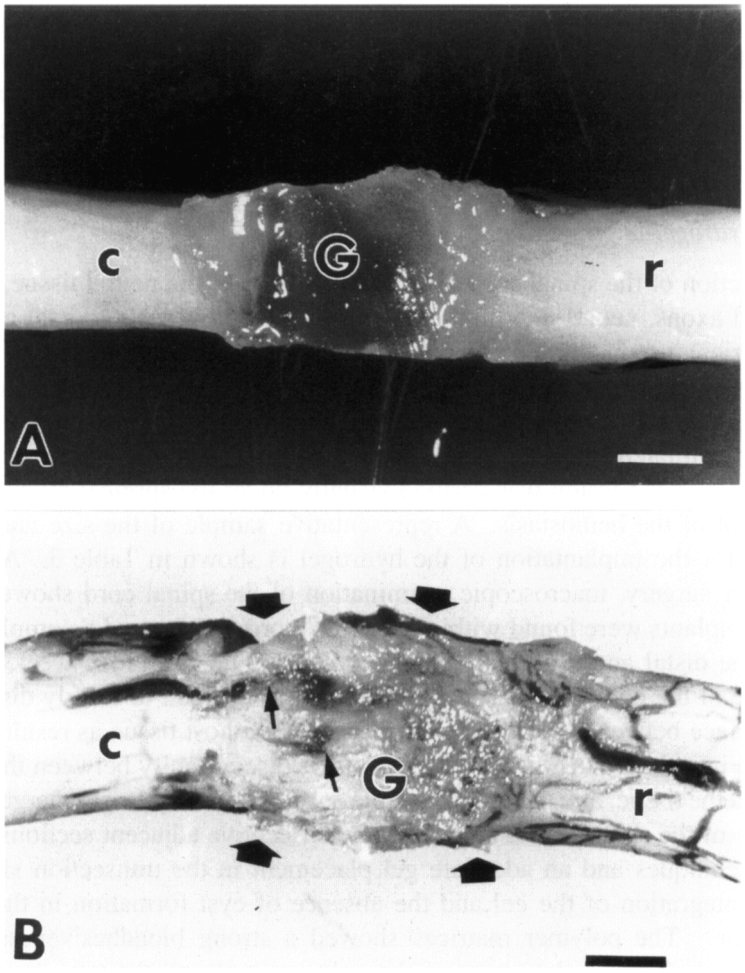

Figure 5. Representative macrophotographs showing the appearance of the transected rat spinal cord grafted with the PHPMA hydrogel after 3 days (A) and 5 weeks (B). Note the fusion of the polymer gel (G) to the rostral (r) and caudal (c) cut end of the cord (arrows) and the restoration of the continuity of the spinal cord (B). (B): note the growth of blood vessels from the cut dorsal spinal artery at the level of the rostral (r) and caudal (c) spinal segments into the polymer gel (small arrows). (C): control spinal cord that did not receive the gel implant, showing degenerative changes of the spinal cord stumps and the fibrous tissue filling the defect (asterix) 5 weeks after transection. Scale bars: (A, B) 1.5 mm; (C) 750 μm.

not reveal any signs of polymer degradation or mechanical disruption as seen under Normansky optics (Fig. 6) and was confirmed by scanning electron microscopy of 5 month-explanted gels (Fig. 7). There was no sign of toxicity, inflammatory or distortion in the surrounding neural tissue.

GFAP immunocytochemistry studies showed that after 3 months of implantation, the gliosis that had developed at the proximal and distal spinal stumps infiltrated the porous structure of the hydrogel and sent processes into the gel implant (Fig. 8).

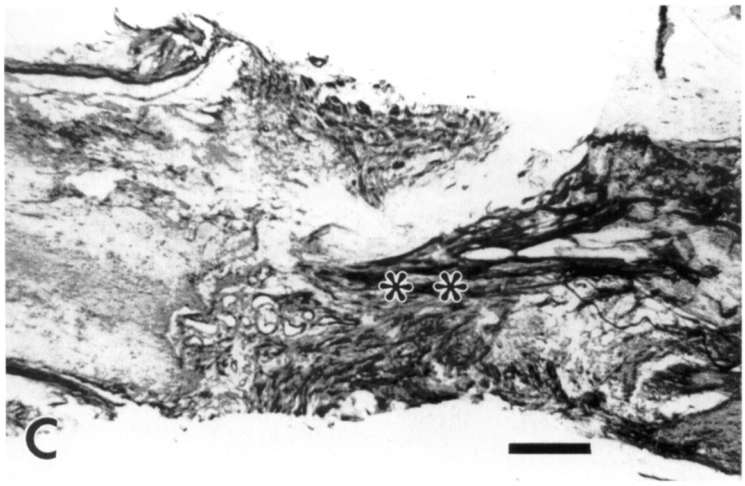

Figure 5. (Continued).

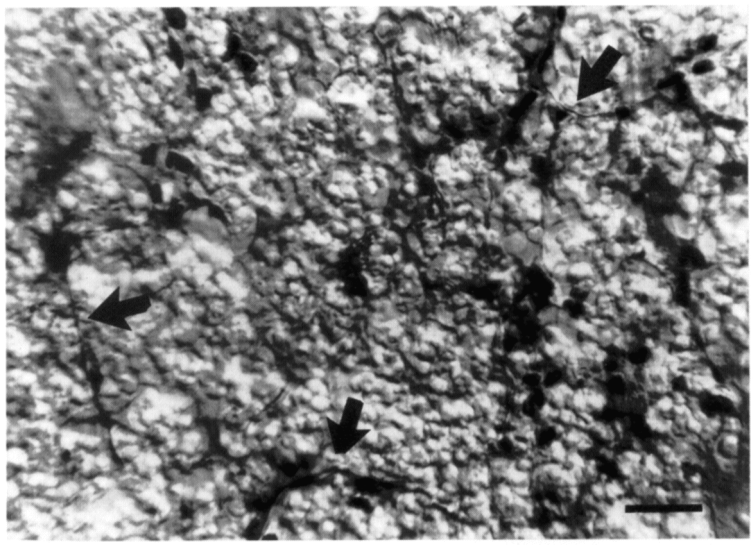

Figure 6. Silver impregnation (Holmes technique) of a section through the hydrogel implant viewed under Normansky optics showing the structure of the gel and nerve fibres between the polymer microspheres (some of them are shown by arrow heads). Scale bar = 15 μm.

This tissue reaction was noticed at the proximal and distal interface and was more pronounced after 20 weeks. Immunostaining with anti-neurofilament antibodies showed intensely stained axons that had crossed the interface and penetrated the gel matrix from the white and gray matter regions of the host (Fig. 9A and B). Twenty weeks after gel implantation, a significant amount of reorganization appeared in the immunoreactive axons at the interface and within the gel matrix. Usually, axons growing within the hydrogel matrices were found in areas which contained astrocytes which have established a network of GFAP-positive processes and blood

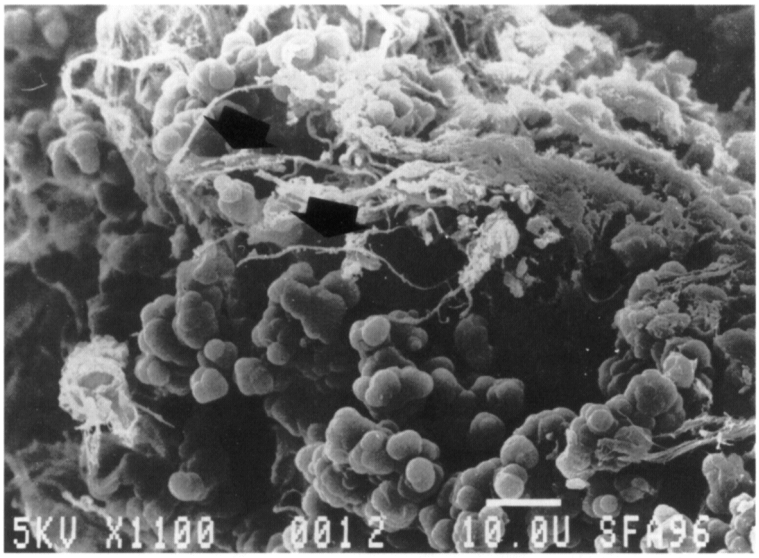

Figure 7. Scanning electron microscopy of the cross-section of a PHPMA gel after 5 months implantation, showing the tissue that has grown within the interstice of the gel and on the surface of the microspheres. Note the structures resembling nerve fibres (arrows).

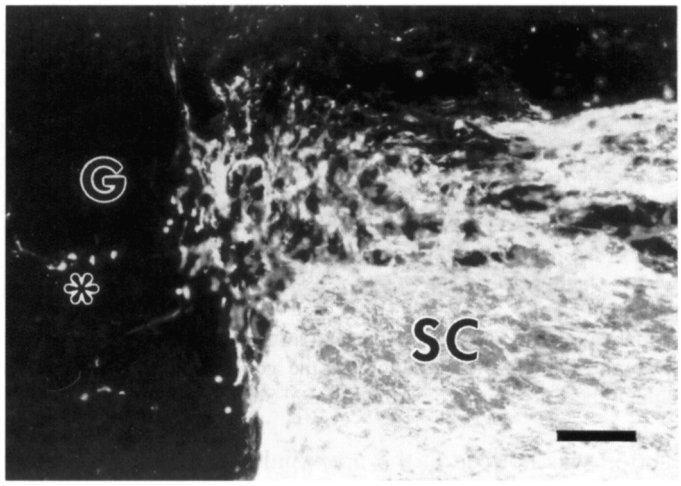

Figure 8. Fluorescent photomicrograph of a longitudinal spinal cord (SC) tissue section (3 months post-implantation) immunostained for glial fibrillary acidic protein (GFAP) showing the gel–tissue interface from the rostral segment of the spinal cord. Astrogliosis occured at the interface and at the level of the spinal stump, while GFAP-positive astrocytes and their processes have spread out into the gel (G). Note the few individual GFAP-positive cells that have detached from the interface and have migrated into the gel (asterix). Scale bar: 100 μm.

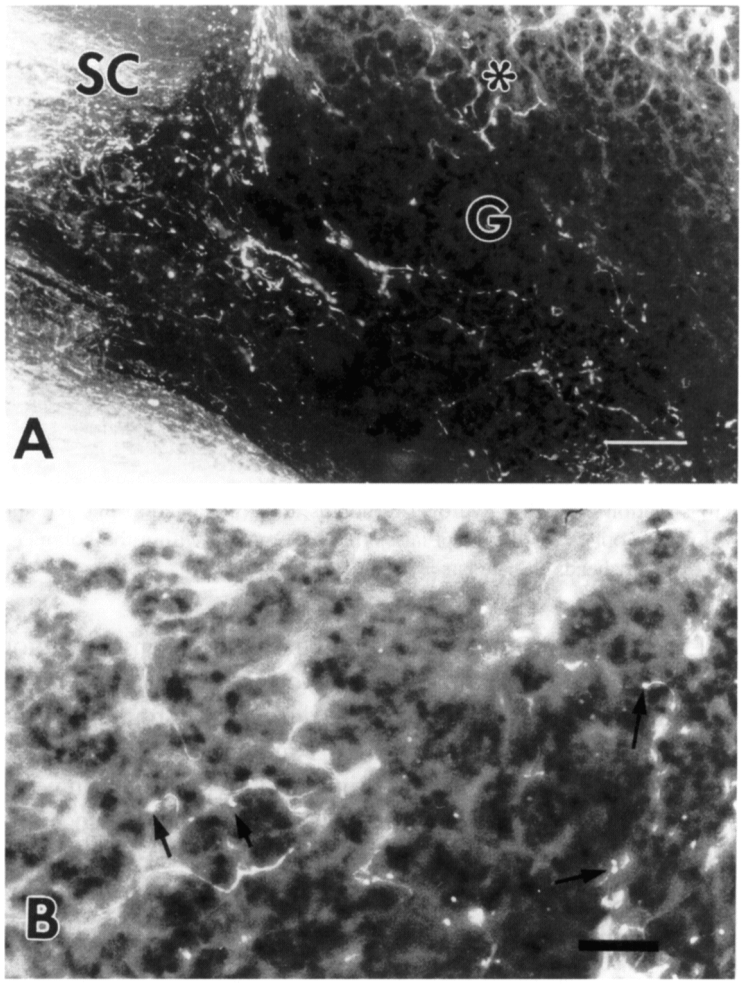

Figure 9. (A) Fluorescent photomicrographs of a longitudinal spinal cord (SC) section (3 months post-implantation) immunostained for neurofilaments showing immunoreactive axons of the white and grey matter of the rostral cut end of the spinal cord. Regenerating fibers have crossed the interface and sprouted (small arrows) within the gel (G) along the trabecular network of the polymer, showing a predominant orientation along the longitudinal axis of the spinal cord. (B) Higher magnification of the area shown by asterix in (A). Very fine diameter axons have grown along different tortuous paths through the porous structure of the gel matrix, mainly as individual fibres displaying ramifications and small terminal varicosities (small arrows). Scale bars: (A) 250 μm; (B) 25 μm.

vessels. Capillary sprouts were constantly observed within the hydrogels (Fig. 10). Immunostaining for fibronectin showed a marked and uniform immunoreactivity of the hydrogel implant and the adjacent tissue (Fig. 11A), and at higher magnification, this immunostaining pattern delineated the microgeometry of the polymer network as a bright and punctuated fluorescence at the surface of the polymer particles (Fig. 11B).

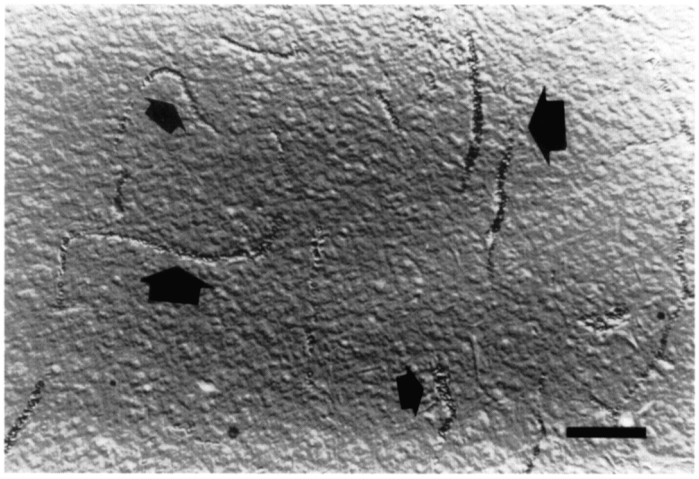

Figure 10. Cross-section through a hydrogel 3 months after implantation into the spinal cord and viewed under Hoffman optics to show capillaries that have grown within the polymer gel (some of them are shown by arrow heads). Scale bar = 20 μm.

Spinal cord sectioning resulted in a loss of reflex and sensory-motor functions below the level of injury. Spontaneous locomotor performance was observed when the rats were allowed to use their hindlimbs during overground locomotion. The differences in locomotor behavior between rats and groups were best seen when the animals were motivated to perform (e.g. stimulation with food). In control groups, the rats were able only to drag their hindlimbs and in some instances were able to perform slight hindlimb joint movements. At 5 weeks post-implantation, the rats grafted with the gel showed significant behavioral improvement compared to the control group with, for instance, extensive movement of all joints of the hindlimbs. However after 5 weeks, improvement was more consistent as all rats regained the ability to take weight-supported steps at least occasionaly during overground locomotion. After 12 weeks post-implantation, six rats stepped consistenly with frequent forelimb-hindlimb coordination and occasional plantar stepping of their hindlimbs, while other rats showed intermediate levels of recovery. No significant improvement was noted for the remaining rats which survived up to 20 weeks.

Figure 12 shows the IR spectra of the hydrated PHPMA control hydrogel and the control (intact) spinal cord, respectively. The IR spectrum of the hydrogel (Fig. 12A) essentially exhibits IR features characteristic of the stretching mode vibration of methylene groups (between 2700 and 3000 cm^{-1}) and of the amide vibrational modes near 1650 (amide I), 1550 (amide II) and 1250 (amide III) cm^{-1}. However, the IR spectrum of the intact spinal tissue (Fig. 12C) shows, despite significant IR absorption due to the presence of water, IR peaks characteristic of proteins as observed by the presence of the amide I (strongly overlapped with the water bending mode feature), amide II and amide III bands. Weak IR peaks are also observed between 2700 and 3000 cm^{-1}, most likely due to the amino acids

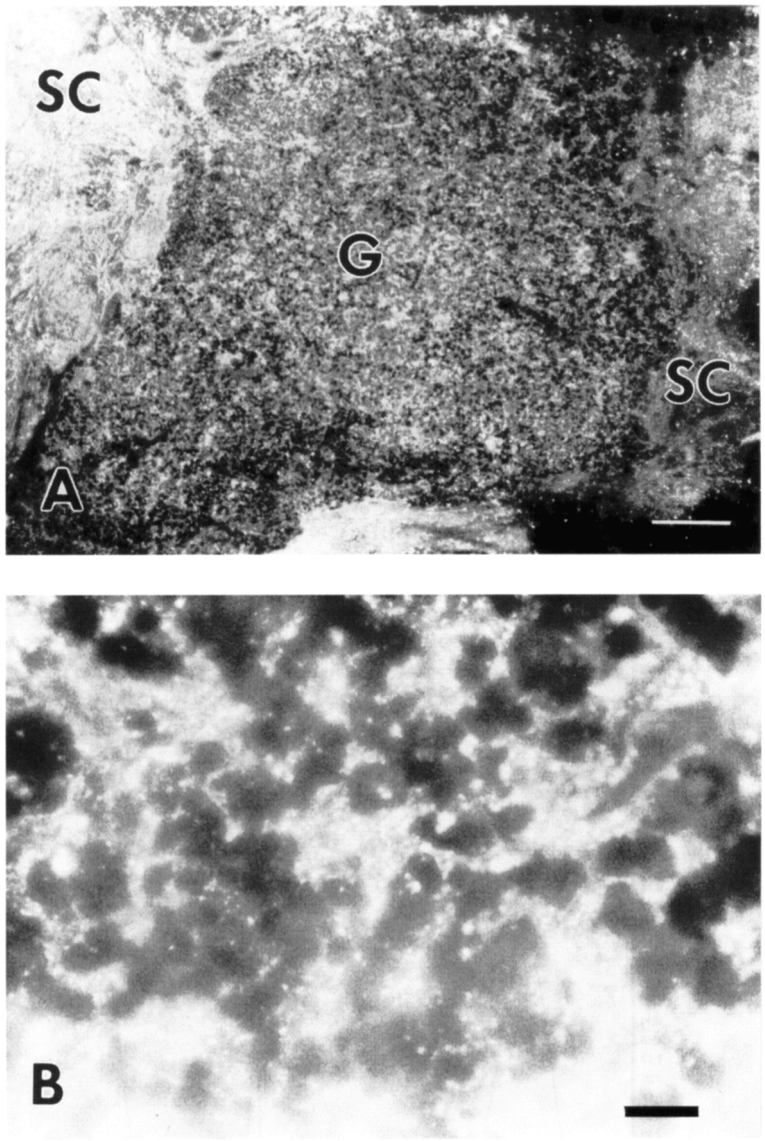

Figure 11. (A) Fluorescent photomicrographs of a longitudinal spinal cord (SC) tissue section (5 months post-implantation) through the implantation site immunostained for fibronectine. (A) At low magnification, the whole hydrogel implant (G) is intensely immunostained and the staining pattern depicts the microgeometry of the gel structure. (B) Higher magnification of the gel showing the punctuated fibronectine staining pattern around the polymer particles. Scale bars: (A) 400 μm; (B) 20 μm.

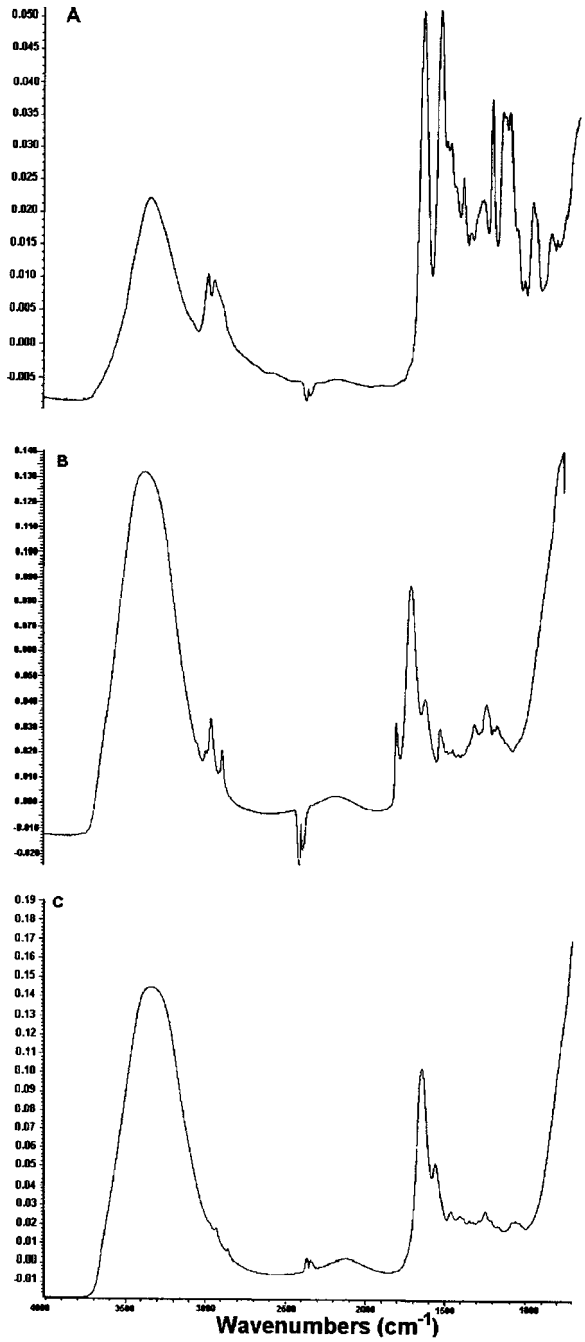

Figure 12. ATR-FTI spectra of a control PHPMA hydrogel (A), a hydrogel explanted after 3 months of implantation in the spinal cord (B), and the intact spinal tissue (C).

side chains. Finally, Figure 12B shows the IR spectra of the explanted PHPMA hydrogel. Interestingly, the low frequency part of the spectrum clearly showed that the hydrogel has been, at least partly, replaced by IR features characteristic of lipids; methyl and methylene stretching mode vibrations between 2700 and 3000 cm^{-1} and ester carbonyl stretching mode vibrations at 1740 cm^{-1} and proteins as similarly observed through the amide bands described above for spinal tissue.

DISCUSSION

The primary goal of this study was to assess the potential of a heterogeneous hydrogel for promoting tissue repair and axonal regeneration in the lesion site of the transected spinal cord. The results show that the hydrogel can correctly bridge the tissue defect, induce glial cell infiltration, angiogenesis and axonal regeneration by recruiting host tissue cells and axons. This study clearly shows differences between the appearance of the spinal cord grafted with the hydrogel and the transected spinal cord without the gel implant. Following severe trauma of the spinal cord, pathological changes occur which are responsible for the progressive necrotizing processes in the spinal stumps [47]. Although the secondary pathological changes may vary considerably according to the severity of the trauma, they include the formation of microcysts and cavitation, formation of a gliomesenchymal scar and tissue necrosis of the gray and white matter in a caudo-rostral extent. In contrast, the spinal cord grafted with the PHPMA hydrogel did not show any such pathological changes. The spinal cord continuity was re-established and, at the microscopic level, the hydrogel was integrated well with the host tissue; on longitudinal sections, fusion of the gel to the host was 100% of the available surface of the polymer implant. Immunocytochemical studies revealed that a major finding of this study was that regeneration of axons within the structure of the polymer hydrogel occurred. The source of regenerating fibers may include: (1) regenerating central axons, either terminal regrowth or collateral sprouting; (2) heterotopic peripheral nerve fibers; (3) proliferating perivascular nerve fibres; (4) regenerating nerve roots [48]. Although intramedullary sprouts from spinal nerve roots, either the posterior root ganglia or the nerve roots themselves, have been reported to be an important source of regenerating fibres [49], it is most likely that axonal regeneration observed through the polymer bridge originates from central axons. This is suggested by the immunocytochemical labbelling patterns which demonstrated that immunoreactive axons originated from the gray and white matter of the proximal and distal spinal segments. In addition, the fact that animals showed some degree of recovery of locomotion and postural functions of the hindlimbs, suggest that timely axonal regeneration occurred when considering that 5–10% of regeneration induce significant functional recovery [50].

Correlation between the performance and the physical characteristics of the hydrogel suggests three levels of control on host tissue response. First, at the macroscopic level (millimetre scale), the high swelling behavior and the viscoelastic

properties of the hydrogel enables the complete sealing of the tissue defect in volume and shape as shown by histopathological studies. Second, on the scale of pore size distribution (micrometric scale and microgeometry), the polymer network control tissue ingrowth as shown by histochemical data and scanning electron microscopy. Finally, at the surface level of the hydrogel (mesoscopic scale), the surface is the site of protein and lipid adsorption as shown by infrared spectroscopy on the explanted hydrogel.

A major issue in tissue engineering using porous polymer devices is the pore size distribution and the communication between pores [51, 52]. In the present study mercury porosimetry and α measurement shows that the PHPMA hydrogel provides a large void volume and an extensive network of interconnected open pores for cell infiltration and tissue growth. Indeed, the intrusion of mercury occurs only within interconnected network of pores which are readily accessible to mercury at increasingly higher pressures [40]. According to porosimetry data and derived equations, the PHPMA hydrogel exhibits a bimodal pore distribution, one in the macropore domain and one in the mesopore domain. It is likely that these domains are occupied by pores with different shapes since the pressure (P) required to intrude a pore volume is inversely proportional to the pore diameter (D) and directly proportional to the shape of the pore (F_s) according to the equation: $P = F_s/D$ [53]. The presence of the two pore regimes is also consistent with scanning electron microscopy which shows the presence of mesopores at the surface of the microspheres ('orange peel' appearance), while the macropores are formed by the interstices between the polymer aggregates. In addition, the macropore domain of the gel encompasses the dimension of the range of biological structures of the spinal tissue that includes capillaries and axons and tissue expansion in the higher limits of the pore size distribution curve. Regarding the topology of the pore network, the gel is formed by a network of pores of variable size with an average diameter D_c, interconnected throughout pore constrictions with an average diameter D_t, since the existence of a hysteresis between the intrusion and retraction curve depends on D_c/D_t [54, 55]. Extrusion data also indicated that pores may trap mercury due to pore irregularities (tortuousness of the network). The large surface area of the polymer network is also a characteristic that promotes tissue formation since cell attachment on a substrate is the initial process in building tissue structure. The value of the surface area of porosimetry data is the area that mercury can reach. However, in this study, this value is underestimated because there is no contribution of the finer mesopores (below 6 mm) and any micropores due to the limit of the pressure range used. However, nitrogen adsorption isotherms have shown a specific surface area of 700 $m^2\,g^{-1}$ for the range of mesopores and micropores of the PHPMA hydrogels (unpublished data).

The high swelling capacity of the gel is a desirable characteristic because it allows transport of nutrient and fluids through the network and modulates the biological processes by controlling diffusion or sequestration of growth factors and cytokines that are secreted after injury [65]. In addition, the gel shows adequate mechanical

integrity (seen upon implantation and rheology) which is important for tissue organization upon the time scale required for tissue morphogenesis, organization and axonal regeneration.

The main results obtained in the rheology study is that the gel exhibits similar mechanical behavior as found in the rat brain. This property is important because it enables the hydrogel to integrate into the neural tissue without mechanical pressure. The fact that G'' does not vanish at low frequencies [56] suggests that the three-dimensional polymer network is not completely cross-linked and local frictions of strands exist in the network. However, the gel was washed several times before rheological measurements, and therefore the friction could only be due to pendant PHPMA chains within the network. In contrast, the elastic modulus G' which is associated with the long scale three-dimensional network response does not show any change in magnitude as expected. Compression and decompression of the gel network is relatively stable whenever submitted to external stresses of the same magnitude as those imposed during the compression/decompression solicitations. Such a property is important when the gel is intended to be subjected to mechanical constraints within the neural tissue.

Since the mechanical properties of soft tissue are related to its structure, it is tempting to speculate on the resemblance between the PHPMA hydrogel and the developing neural tissue which has relatively large extracellular spaces, representing a significant volume fraction [57]. In early postnatal days the TMA^+ diffusion parameters in a rat cortex and corpus callosum are significantly different from those in adults. The extracellular space volume fraction α in a newborn rat is more than twice as large (about 0.45) than it is in the case in an adult rat brain (about 0.20) [57] and the tortuosity during early postnatal days is significantly lower [58]. Recently, the similar decrease in α and increase in λ were demonstrated in the developing rat spinal cord gray and white matter [60]. For instance, the neural tissue and the PHPMA hydrogel both can be viewed as composed of a deformable porous matrix saturated by interstitial fluids. In the case of the neural tissue, the solid phase is made up of extracellular matrices and the vascular network, and the fluid phase, of the extra- and intracellular fluids. The hydrogel after implantation, can, nevertheless, be viewed as composed of a solid elastic phase, the polymer matrix, and a fluid phase; the biological fluid as described with the poroelastic model [60, 61].

The hydrogel upon implantation interactes closely with the host tissue as evidence by scanning electron microscopy and infrared spectroscopy, showing clearly that the PHPMA hydrogel is invaded by tissue cells, while lipids and protein molecules are adsorbed on the polymer surface. Lipids adsorption may be residual myelin debris or newly formed myelinated axons that have grown on polymer surfaces (however, further immunocytochemical analysis is needed). Adsorption could have been favored by the amide functionality of the PHPMA which confers stability and polarity of the network [62]. Adsorption of extracellular matrix proteins onto polymer surfaces is substantiated by immunocytochemistry of fibronectin that showed a very fine fluorescent signal depicting the microgeometry of the polymer

matrix. This very likely contributes to the attachment and the growth of cells onto the polymer surface as shown in other studies (e.g. [63]).

The present study also shows the importance of the surgical technique used to implant the hydrogel into the lesion cavity. For instance, proximal and distal interfaces free of mesenchymal debris and blood are conditions for apposition of the hydrogel to the traumatic spinal surfaces. Indeed, the quality of the two surfaces (biologic vs synthetic) that come into contact is important for the fate of the integration process of the hydrogel and tissue induction. Indeed, formation of cysts and scarring tissue occur after excessive manipulation of the spinal tissue that results in the failure of the hydrogel function in tissue restoration.

As early as 1990, tissue repair using synthetic polymer hydrogel was suggested as a new strategy for brain tissue repair [29, 30]. Homogeneous transparent hydrogels of glyceryl methacrylate or hydroxyethyl methacrylate have been studied as polymer matrices for tissue replacement in the CNS but were less effective to integrate the neural tissue than the heterogeneous hydrogel in the present study. The neuroinductive property of the PHPMA hydrogel is a function of the water content of the network which facilitates the diffusion of biological fluids and growth factors secreted by cells, the mechanical compliance and adequate integrity to host tissue, the large specific surface area available for tissue interaction and organization, and the porous structure with a median pore diameter compatible with cell infiltration. Other polymer systems that have been used to promote tissue regeneration are different from the hydrogel of this study because they form tubes without three-dimensional tissue structure [23] or are synthesized from biodegradable polymer [28]. Biodegradable materials present disadvantages because their side products released into the systemic circulation may cause, over the long term, organ failure by accumulation into the tissue. In contrast of the present study, heterogeneous hydrogels of poly(2-hydroxyethyl methacrylate) combined with collagen and Schwann cells were tested in the rat brain, showing some degree of tissue ingrowth [32].

Following trauma of the spinal cord, healing of the lesion and the surrounding tissue is the result of two apparently independent processes of tissue necrosis and tissue repair [64]. The aim of neural tissue engineering using polymer hydrogels is to regulate the dynamic balance between these two processes by providing the appropriate substrate to promote the naturally occurring reparative events which may overwhelm the wound healing. These reparative events include the development of a cellular matrix, the secretion of extracellular matrices, axonal sprouting and delivery of growth and angiogenic factors. The ultimate goal is not to recreate a replica of the lost tissue with its original anatomical organization including minute structural features, topographic cell distribution and specific arrangement of dendritic and axonal processes, but to restore the lost tissue with the host cell elements arranged collectively into a level of structural organization that promotes axonal regeneration and the establishment of new neural connections.

In this respect, reactive astrocytes by producing growth-promoting proteins and neurotrophic factors can be beneficial for axonal regeneration [65].

Tissue engineering of the nervous system is a relatively new field of research compared to other organs but, with advanced knowledge in the molecular biology of CNS development and regeneration, materials tailored for reconstituting the CNS tissue will be manufactured. For instance, one of the future challenges will be to control topologically the modification of polymer matrices with bioactive functional groups chemically grafted to the polymer [66, 67]. Another approach that is being developed is the association of hydrogels with developing cells that may further expand within the porous polymer network [68–71] to construct biohybrid implants for tissue replacement.

CONCLUSION

The present finding shows that a biocompatible macroporous polymer hydrogel with defined pore structure and topology that are potentially available for tissue development, and associated tissue-compatible mechanical properties have the capacity to induce and support neural tissue ingrowth and axon regeneration. Engineering the neural tissue based on hydrogel technology has future applications in microreconstruction neurosurgery in the restoration of defective tissue (gliotic scar resection), tissue destruction (trauma) or dysfunctional tissue (spina bifida).

Acknowledgements

We express our thanks to Mrs. Suzanne Bourassa for technical assistance and Dr. R. Guidoin (Quebec Biomaterial Institute) for the use of the scanning electron microscope.

REFERENCES

1. B. A. Kakulas and J. R. Taylor, in: *Handbook of Clinical Neurology*, H. L. Frankel (Ed.), p. 21. Elsevier Science (1992).
2. A. Larner, A. R. Johnson and R. J. Keynes, *Biol. Rev.* **70**, 597 (1995).
3. A. Logan, J. Oliver and M. Berry, in: *Progress in Growth Factor Research*, Vol. 5, p. 379. Elsevier Science, Oxford (1995).
4. J. S. Rudge, G. M. Smith and J. Silver, *Exp. Neurol.* **103**, 1 (1989).
5. E. L. Zager and McL. P. Black, *Surg. Neurol.* **29**, 350 (1988).
6. O. Lindvall, *J. Neurol. Neurosurg. Psychiatry*, supp., 39 (1989).
7. B. S. Bregman, *Dev. Brain Res.* **34**, 265 (1987).
8. K. R. Kuhlengel, M. B. Bunge, R. P. Bunge and H. Burton, *J. Comp. Neurol.* **293**, 74 (1990).
9. J. J. Bernstein and W. J. Goldberg, *Rest. Neurol. Neurosci.* **2**, 261 (1991).
10. O. Brustle and R. D. McKay, *Curr. Op. Neurobiol.* **6**, 688 (1996).
11. C. N. Svendsen, M. A. Cadwell, J. Shen, M. G. Borg, A. E. Rosser, P. Tyers, S. Karmiol and S. B. Dunnett, *Exp. Neurol.* **148**, 135 (1997).
12. A. Martinez-Serrano and A. Bjorklund, *Trends Neurosci.* **20**, 530 (1997).

13. J. R. Wrathall, D. D. Rigamonti, M. R. Bradford and C. C. Kao, *Acta Neuropathol.* **57**, 59 (1982).
14. J.-C. Horvat, C. Baillet-Derbin, J. H. Ye, F. Rhrich and F. Affane, *Rest. Neurol. Neurosci.* **2**, 289 (1991).
15. R. Marchand and S. Woerly, *Neuroscience* **36**, 45 (1990).
16. E. A. Joosten, P. R. Bar and W. H. Gispen, *J. Neurosci. Res.* **41**, 481 (1995).
17. H. S. Goldsmith and J. C. de la Torre, *Brain Res.* **589**, 217 (1992).
18. Y. Hiraizumi, E. Fujimaki, E. E. Transfeld, N. Kawahara, V. D. Fiegel, D. Knighton and J. H. Sung, *Spinal Cord* **34**, 394 (1996).
19. J. J. Bernstein and W. J. Goldberg, *Brain Res.* **377**, 403 (1986).
20. C. L. Paino, C. Fernandez-Valle, M. L. Bates and M. B. Bunge, *J. Neurocytol.* **23**, 433 (1994).
21. M. H. Spilker, I. V. Yannas, H.-P. Hsu, T. V. Norregaard, S. K. Kostyk and M. Spector, *Tissue Eng.* **3**, 309 (1997).
22. D. J. Schreyer and E. G. Jones, *Dev. Brain Res.* **35**, 291 (1987).
23. X. M. Xu, V. Guénard, N. Kleitman and M. B. Bunge, *J. Comp. Neurol.* **351**, 145 (1995).
24. M. S. Shoichet, S. R. Winn, S. Athavale, J. M. Harris and F. T. Gentile, *Biotechnol. Bioeng.* **43**, 563 (1994).
25. C. T. Montgomery, E. A. Tenaglia and J. A. Robson, *Exp. Neurol.* **137**, 277 (1996).
26. A. R. Harvey, M. Chen, G. W. Plant and S. E. Dyson, *Rest. Neurol. Neurosci.* **6**, 221 (1994).
27. A. R. Harvey, A. M. Connor and M. W. Beilharz, *Int. J. Dev. Neurosci.* **11**, 569 (1993).
28. C. Shugens, C. Grandfils, R. Jerome, P. Teyssie, P. Delree, D. Martin, B. Malgrange and G. Moonen, *J. Biomed. Mater. Res.* **29**, 1349 (1995).
29. S. Woerly, C. Lavallée and R. Marchand, *Biomaterials* **11**, 97 (1990).
30. S. Woerly, K. Ulbrich, V. Chytry, K. Smetana, P. Petrovicky, B. Rihova and D. J. Morassutti, *Cell Transplant* **2**, 229 (1993).
31. S. Woerly, *Biomaterials* **14**, 1056 (1993).
32. G. W. Plant, A. R. Harvey and T. V. Chirila, *Brain Res.* **671**, 119 (1995).
33. N. A. Peppas (Ed.), *Hydrogels in Medicine and Pharmacy*. CRC Press, Boca Raton, FL (1987).
34. J. D. Andrade (Ed.), *Hydrogels for Medical and Related Applications*, ACS Symp. Ser. 31. ACS, Washington, DC (1976).
35. K. Dusek, *J. Polym. Sci. B* **3**, 209 (1965).
36. J. Seidl, J. Malinsky, K. Dusek and W. Heitz, *Adv. Polym. Sci.* **5**, 113 (1967).
37. J. Strohalm and J. Kopecek, *Angew. Makromol. Chem.* **70**, 109 (1978).
38. J. L. Nation, *Stain Technol.* **58**, 347 (1983).
39. E. W. Washburn, *Proc. Natl Acad. Sci. USA* **7**, 115 (1921).
40. S. J. Gregg and K. S. W. Sing (Eds), *Adsorption, Surface Area and Porosity*. Academic Press, London (1982).
41. M. Shively, *J. Pharmaceutical Sci.* **80**, 376 (1991).
42. Bird, R. C. Armstrong and O. Hassager, *Dynamic of Polymeric Liquids*. J. Wiley, New York (1987).
43. E. Sykova, J. Svobova, J. Polak and A. Chvatal, *J. Cereb. Blood Flow Metab.* **14**, 301 (1994).
44. C. Nicholson and J. M. Phillips, *J. Physiol.* **321**, 225 (1981).
45. E. Sykova, *The Neuroscientist* **3**, 28 (1997).
46. M. Bousmina and R. Muller, *Rheol. Acta* **35**, 369 (1996).
47. D. Balentine, *Lab. Invest.* **39**, 236 (1978).
48. L. Wolman, *Paraplegia* **4**, 175 (1966).
49. J. Komon, M. Van Meter, S. Salzman and W. Young, *Exp. Neurol.* **148**, 453 (1997).
50. A. R. Blight, *Neuroscience* **10**, 521 (1983).
51. E. Wintermantel, J. Mayer, K. L. Eckert, P. Lüscher and M. Mathey, *Biomaterials* **17**, 83 (1996).
52. R. C. Thomson, M. C. Wake, M. J. Yaszemski and A. G. Mikos, *Adv. Polymer Sci.* **122**, 245 (1995).
53. O. Z. Cebeci, *J. Colloid Interface Sci.* **78**, 383 (1980).

54. C. D. Tsakiroglou and A. C. Payatakes, *J. Colloid Interface Sci.* **137**, 315 (1990).
55. F. A. Dullien and G. K. Dhawan, *J. Colloid Interface Sci.* **47**, 337 (1974).
56. W. M. Abbot and R. P. Cambria, in: *Biological and Synthetic Vascular Prostheses*, J. C. Stanley *et al.* (Eds), p. 189. Grune & Stratton, New York (1989).
57. A. Lehmenkühler, E. Sykova, J. Svoboda, K. Zilles and C. Nicholson, *Neuroscience* **55**, 339 (1993).
58. I. Vorisek and E. Sykova, *J. Cereb. Blood Flow Metab.* **17**, 191 (1997).
59. S. Prokopova, L. Vargova and E. Sykova, *Neuroreport* **8**, 3527 (1997).
60. T. Nagashima, N. Tamaki, S. Matsumoto, B. Horwitz and Y. Seguchi, *Neurosurgery* **21**, 898 (1987).
61. S. Hakim, *Acta Neurol. Latinoam.* **17**, 169 (1971).
62. S. Dumitriu and C. Dumitriu-Medvichi, in: *Polymeric Biomaterials*, S. Dumitriu (Ed.), p. 3. Marcel Dekker, New York (1993).
63. S. T. Carbonetto, M. M. Gruver and D. C. Turner, *Science* **216**, 897 (1982).
64. Z. Zhang, C. J. Krebs and L. Guth, *Exp. Neurol.* **143**, 141 (1997).
65. H. W. Muller, U. Junghans and J. Kappler, *Pharmacol. Ther.* **65**, 1 (1995).
66. G. W. Plant, S. Woerly and A. R. Harvey, *Exp. Neurol.* **143**, 287 (1997).
67. S. Woerly, G. Laroche, R. Marchand, J. Pato, V. Subr and K. Ulbrich, *J. Neural Transpl. Plast.* **5**, 245 (1995).
68. S. Woerly, G. W. Plant and A. R. Harvey, *Neurosci. Lett.* **205**, 197 (1996).
69. S. Woerly, G. W. Plant and A. R. Harvey, *Biomaterials* **17**, 301 (1996).
70. C. E. Krewson, S. W. Chung, W. Dai and W. M. Saltzman, *Biotechnol. Bioeng.* **43**, 555 (1994).
71. A. C. Jen, M. C. Wake and A. G. Mikos, *Biotechnol. Bioeng.* **50**, 357 (1996).